DOI: 10.21062/mft.2022.038 http://www.journalmt.com

Theoretical and Experimental Study on the Influence of Ultrasonic Vibration on Contact Friction

Changli Zha (0000-0003-2141-642X), Shenlong Zha (0000-0002-0063-2775)
School of Electronic Engineering and Intelligent Manufacturing, Anqing Normal University, Anqing, Anhui, China 246133. E-mail: 504275049@qq.com

The effects of punch radius, deep-drawing speed and amplitude on the friction coefficient were studied on an improved drawing-bulging friction coefficient testing device on basis of ultrasonic vibration. A contact friction model based on the tribology theory of adhesion and plowing was constructed and used to explain the friction reduction phenomenon of applied out-of-plane normal vibration. The results show that the friction coefficient decreases with the increase of ultrasonic vibration amplitude. At the same deep-drawing height, the friction coefficient decreasing rates at amplitude of 7.8um and 10.1 um on the deep-drawing speed of 0.1 mm/s and 10 mm/s, were 6.7% and 18.8%, respectively. The friction coefficients at the punch radii R0.3 and R1.5 declined from 0.18 to 0.13 and from 0.12 to 0.11. The friction coefficients of thin specimens were larger than thick specimens whether ultrasonic vibration was applied or not. The average friction coefficient from theoretical modeling (μ_v) was smaller than the friction coefficient without ultrasonic vibration (μ_0), and the relative friction coefficient ratio declined with the rise of amplitude and was inversely proportional to time.

Keywords: Ultrasonic vibration, Friction coefficient, Surface effect, Drawing-bulgin, Surface morphology

1 Introduction

Ultrasonic vibration-assisted metal plastic forming can effectively decrease forming force and contact friction and improve surface quality of formed parts. Therefore, ultrasonic vibration is applied to plastic forming processes, such as stamping [1], [2], [3], wire drawing [4], [5], upsetting [6] and other technical fields [7], [8], [9], [10]. Since micro plastic metal forming is different from metal macro-forming, friction directly affects the forming properties and quality of formed metal parts. Hence, the friction during micro-forming processes has been a research hotspot. Experimentally, Siegert et al. applied ultrasonic vibration into a strip-drawing process to study the effects on friction and found the decrease of frictional force and the improvement of surface quality were both associated with the vibration amplitude and deep-drawing speed [11]. Ngaile and Bunget probed into extrusion microforming of aluminium materials and copper materials and noticed that the surface quality of formed parts was obviously improved under ultrasonic vibration [12]. During micro-upsetting experiments, ultrasound significantly affected surface roughness, which considerably dropped from 1.376 to 0.77 after the application of ultrasonic vibration [13]. Hung et al. determined friction calibration curves and friction factors through the finite element method through upsetting experiments on the ring compression of aluminum alloys, and further quantitatively analyzed the relation between friction coefficient and ultrasonic vibration through double-cup extrusion experiments, which showed ultrasonic vibration significantly affected the friction factor [14]. Moreover, at the theoretical level, the existing research is focused on in-plane and out-of-plane aspects. Tsai et al. proposed a theoretical method based on the Dahl friction model and found friction was lowered when tangential vibration occurred at any in-plane angle [15]. The theoretical and Experimental Research on the effect of in-plane and out-of-plane vibration on friction, such as the work done by Popov et al., have been carried out systematically [16], [17], [18], [19]. Teidelt et al. theoretically studied the effects of out-of-plane normal ultrasonic vibration on static friction and slide friction [20]. The above studies empirically underlie the qualitative interpretation and analysis concerning the effects of ultrasonic vibration on contact friction, but the results of theoretical models and experiments are inconsistent to some extent.

For this reason, a frictional property testing device about SUS304 sheets under ultrasonic vibration was designed and used to simulate the friction status during practical deep-drawing forming. The friction coefficients of specimens with different thicknesses, mould dimensions, deep-drawing speeds and amplitudes during drawing-bulging were studied. The effects of thickness, mould, deep-drawing speed and amplitude on friction coefficient were analyzed. At the same time, a contact friction model based on the tribology theory of adhesion and plowing was constructed and used to explain the friction reduction

phenomenon of applied out-of-plane normal vibration. Together with experimental results, relevant parameters of the theoretical model were calibrated and used to analyze modeling precision.

2 Drawing-bulging experiment

Metal sheet drawing-bulging experiments under ultrasonic vibration for friction coefficient measurement were conducted to investigate the effects of specimen sizes, deep-drawing speed and punch radius on contact friction force, or namely the variation of friction coefficient. In practice, however, the friction coefficient of metal plastic forming is affected by many factors, including stamping velocity, mould dimension parameters, lubrication status, and temperature. To display the actual metal plastic forming as much as possible, we modified the traditional drawing-bulging friction coefficient measurement method and built a metal sheet drawing-bulging friction coefficient measurement platform based on ultrasonic vibration and used it to evaluate contact friction. During drawing-bulging experiments, a metal sheet passed two cylindrical friction heads fixed below the lower mould, and the two ends of the sheet were fixed on the upper mould. The punch formed from deep drawing was simulated through the two cylindrical friction heads, and the diameters of the friction heads were changed to alter the punch radius. Under external loading, the upper mould moved upwards, so the middle segment and the straight wall segment on the metal sheet generated different strains, and then the tensile forces at the two segments were calculated separately. Finally, the average friction coefficient on the contact surface was computed. In actual deep-drawing forming, however, deep drawing and bending occur simultaneously. Hence, Wang et al. modified the drawing-bulging measuring method by adding the contact between cylindrical friction heads and metal specimens, and simulated the co-occurrence of deep drawing and bending through a progressive contact form or namely with the contact angle gradually rising from zero [21]. Our experiment platform was based on the modified method of Wang et al., but we replaced the cylindrical friction heads with punch with varying radius. The deep-drawing forming was realized by the downward movement of punch. The working principle was illustrated in Fig. 1.

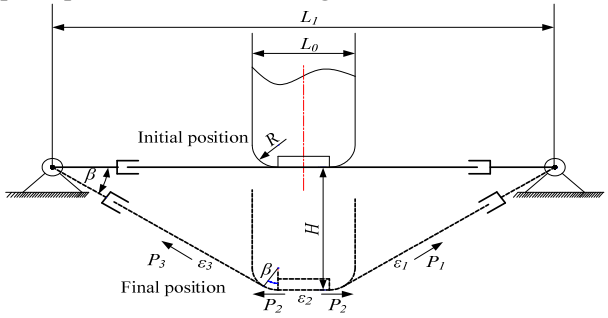

Fig. 1 *Schematic illustration of the friction coefficient testing device*

The metal sheet drawing-bulging friction coefficient measurement platform based on ultrasonic vibration is illustrated in Fig. 2. This platform consists of a CMT4203 electronic universal tensile testing machine, an ultrasonic generator, an ultrasonic transducer, concentrator, clamping parts, force sensors, digital display, and upper pressure head (punch).

To simulate the effects of punch radius on friction during actual deep-drawing forming, we designed punch with varying sizes in a modularized way for friction coefficient measurement. To avoid the interference of contact between specimens and punch lower surfaces, we concaved the lower surfaces of punch. In the meantime, to avoid the interference from the substances attached to the punch and from the impurities inside the punch, we precisely ground and polished the punch. The real object of a punch is shown in Fig. 3.

Fig. 2 *Friction coefficient testing device*

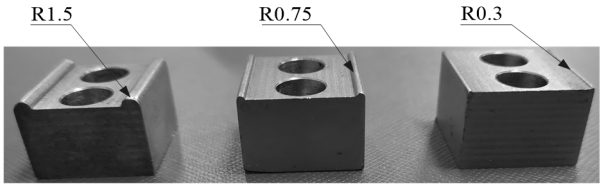

Fig. 3 *Upper pressure head (punch)*

The effects of deep-drawing speed, specimen thickness and amplitude on the friction coefficient were studied. The concrete working parameters were listed in Tab.1. The rated excited frequency of the ultrasonic generator was 19.891 kHz, and its peak power output was 2 kW. The specimens were polished, cleaned, and made into surface printed grids by an electrochemical corrosion method. The grid dots were in diameter of 1 mm and distance of 2 mm. The long axis and short axis strains of each grid dot after deformation were measured using an electron microscope. The specimen working sizes and the real object after gridding were shown in Fig. 4. During the experiments, each specimen was repeated at least 3 times under each scheme, which ensured the effectiveness of the experimental results.

Tab. 1 *Experimental parameters of friction coefficient measurement*

Parameters	value
Drawing speed（mm/s）	0.1 10
thickness（mm）	0.1 0.2
Vibration amplitude（um）	3.9 7.8 10.1

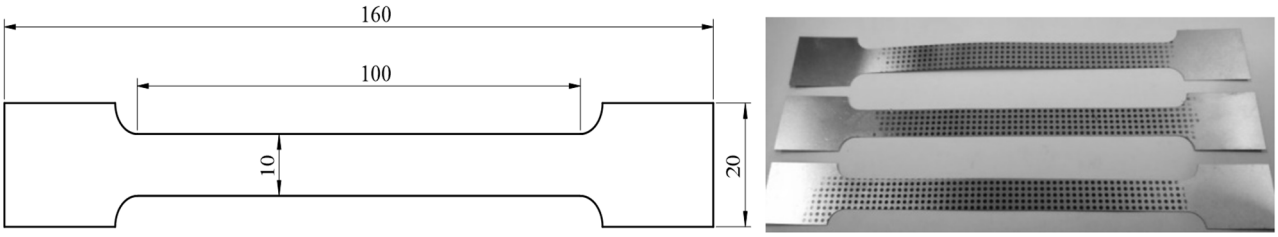

a) the size of specimen/mm *b) specimen with printed grid*

Fig. 4 *The shape and size of SUS304 specimen/mm*

According to the friction coefficient measurement principle (Figure 1), the pulling forces P1 and P3 at the left and right straight parts of each specimen were measured using a force sensor, and the measured data were fed back to digital display. Then P1=P3 was adjusted according to structure principle and force balance. The pulling force P2 at the middle of each specimen was determined indirectly: the long axis and short axis strains of each printed grid dot after deformation were measured firstly, then the corresponding stress was determined according to the tensile stress strain curve of SUS304 and finally [22], P2 was calculated according to a function. Hence, P2 can be computed as follows:

$$P_2 = \sigma_1 wt \ , \tag{1}$$

Where:

σ_1…Instant principal stress,

w…Specimen width,

t…Specimen thickness.

At this time, the friction coefficient was calculated as follows[23]:

$$\mu_e = \frac{1}{\beta} \ln \frac{P_1}{P_2}, \tag{2}$$

Where:

B…Contact wrap angle between a specimen and a punch and it varies with the change of punch stroke and meets the following equation:

$$A\sin\beta + B\cos\beta = 1 \ , \tag{3}$$

At $0 \le \beta \le \frac{\pi}{2}$, we have $A = \frac{L_1 - L_0 + 2R}{2R}$ and $B = \frac{R-H}{R}$. Then β can be determined according to the punch stroke H.

The friction coefficients at varying punch radius (R0.3/ R0.75/ R1.5) and at the experimental parameters in Tab.1 were measured, and the effects of each parameter on the friction coefficients were analyzed.

3 Theoretical approach

During analysis and research on applied in-plane vibration, it is generally hypothesized that the contact friction coefficient and normal force are both constant. With the applied out-of-plane vibration, the normal force periodically changes, the real sliding velocity also fluctuates at a certain amplitude, and the slide displacement is related to time in a fluctuating way, which is called stick slip. Moreover, it is deduced from the acoustic softening effect that the contact surface is also affected by acoustic softening, so the contact surface possesses more micro asperities plasticity and is more easily flattened, leading to the enlarged contact surface area and smaller friction coefficient and average friction force [24].

The applied out-of-plane vibration induced a periodical fluctuation of normal force, and the resulting instant friction force $F_f(t)$ also periodically changed Figure 5). The object was imposed by the normal load F_N, the contact surface friction coefficient was μ_0, and the constant driving force was F_d. With one vibration period at the stage of $t_1 \le t \le t_2$ or namely when the driving force F_d surpassed static friction force, the two surfaces slipped relatively, forming the instant sliding friction force $F_f(t) = \mu_0 F_N(t)$. At $t_2 < t$ or namely when the driving force F_d was smaller than the static friction force, the two surfaces stuck relatively, forming the sliding friction force $F_f(t) \neq \mu_0 F_N(t)$. The kinematic relation based on the out-of-plane ultrasonic vibration on two interactive surfaces is shown in Fig. 6.

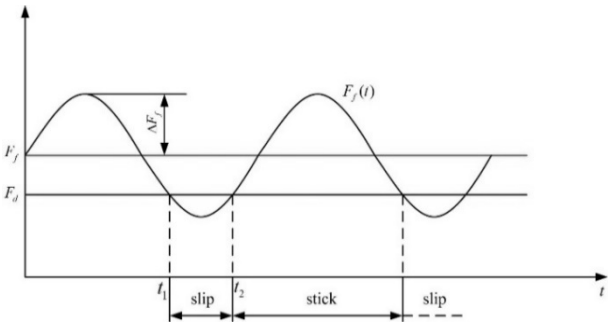

Fig. 5 *State diagram of driving force and instantaneous friction*

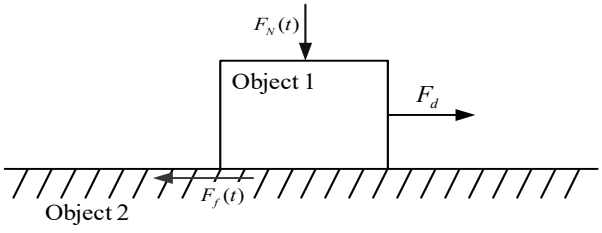

Fig. 6 *Object motion relationship based on out-plane ultrasonic vibration*

Microscopically, the body surface is composed of randomly-distributed micro-convexes, so the real contact area between two surfaces (S_r) is smaller than the theoretical contact area (S_t), but during theoretical analysis, the two are approximately considered as being equal. Hence, the real area can be expressed as:

$$S_r = \frac{F_{N,0}}{H}, \quad (4)$$

Where:

$F_{N,0}$…Normal load without ultrasonic vibration,

H…Hardness of the relatively soft material between two contact surfaces. After the out-of-plane ultrasonic vibration was applied, the normal force or namely the periodical wave force $F_N(t)$ can be written as equation (4), and the real instant contact area S_v is:

$$S_v = \frac{F_N(t)}{H}, \quad (5)$$

Where the periodically fluctuating normal force is:

$$F_N(t) = F_{N,0} + \Delta F, \quad (6)$$

Where:

ΔF…Stress increment induced by the out-of-plane normal ultrasonic vibration. The ΔF can be calculated as:

$$\Delta F = k_t \cdot \xi \cdot \cos(\omega t), \quad (7)$$

Where:

k_t…Normal hardness of the relatively soft material between two contact surfaces,

ξ…Amplitude,

ω…Vibration angular frequency.

According to the tribology theory of adhesion and plowing, when two rough contact surfaces relatively slip, the top of the hard-surface rough micro asperities causes furrows on the soft surface, and the plowing resistance is namely the friction force, which consists of shear stress (τ_s) and plowing force (τ_h). Hence, the friction force is:

$$F_f(t) = S_v(\tau_s + \tau_h), \quad (8)$$

It is generally believed that $\tau_s \gg \tau_h$, so the friction force can be approximated as:

$$F_f(t) = S_v \cdot \tau_s, \quad (9)$$

By combining equations (5) to (8), we can determine the instant friction force:

$$F_f(t) = \frac{F_{N,0} + k_t \cdot \xi \cdot \cos(\omega t)}{H} \cdot \tau_s, \quad (10)$$

Research on the volume effect shows that ultrasonic vibration can cause acoustic softening, leading to a decrease of yield strength [25]. Since yield strength is associated with shear strength, the shearing strength (τ_s) declines and the decreased level of shearing strength is proportional to the amplitude, or namely the shearing strength under vibration (τ_v) can be calculated as:

$$\tau_v = \tau_s - \alpha\xi, \quad (11)$$

Where:

α…Parameter related to the acoustic softening effect. Thus, the instant friction force based on the acoustic softening effect can be determined as:

$$F_{fs}(t) = \frac{F_{N,0} + k_t \cdot \xi \cdot \cos(\omega t)}{H} \cdot (\tau_s - \alpha\xi), \quad (12)$$

According to the theory of adhesion and plowing slide friction of F.P.Bowden and D,Tabor, the contact micro-areas is under a plastic flow state, and the instant high temperature generated during friction causes the metals to stick, forming an stick force[26]. Then under the friction force, the stick micro-areas is overcome to cause cutting slip, or namely the slide friction is the leap of stick-slip alternation. After the application of the out-of-plane normal vibration, the slide friction may be under a stick slip state (Fig. 5). Thus, the friction force theoretical model was analyzed from two states of stick and slip.

At slip stage ($t_1 \le t \le t_2$), the friction at the slip stage was characterized by slide friction, and slip started at t_1 and ended at t_2, and the instant friction force can be expressed as Equation (11). Then the total average friction force within one vibration period was calculated as:

$$\overline{F_{f\_slip}} = \int_{t_1}^{t_2} F_{fs}(t)\,dt, \quad (13)$$

When in the stick stage ($t_2 < t$), the shear stress at the stick stage (τ_v) can be approximated as a linear change. Thus, the instant friction force at this stage can be calculated as:

$$F_{f\_stick}(t) = F_{fs}(t_2) + F_{fs}(t) \cdot (t - t_2), \quad (14)$$

The total average friction force within one vibration period was calculated as:

$$\overline{F_{f\_stick}} = \int_{t_2}^{\frac{2\pi}{\omega}+t_1} F_{f\_stick}(t)\,dt, \quad (15)$$

In all, the average friction force within one period was calculated as:

$$\langle F_{fs} \rangle = \frac{\omega}{2\pi}(\overline{F_{f\_slip}} + \overline{F_{f\_stick}}), \quad (16)$$

The average periodical normal force under out-of-plane normal vibration $F_N(t)$ within one period was:

$$\langle F_N \rangle = \frac{\omega}{2\pi}\int_0^{\frac{2\pi}{\omega}} F_N(t)\,dt, \quad (17)$$

Thus, the friction coefficient under ultrasonic vibration was:

$$\mu_v = \frac{\langle F_{fs} \rangle}{\langle F_N \rangle}, \quad (18)$$

The vibration-free normal force was $F_{N,0}$ and the shear stress was τ_s. Based on equations (4) and (7), the vibration-free friction coefficient was $\mu_0 = \frac{\tau_s}{H}$, and the ratio to the friction coefficient under ultrasonic vibration was:

$$\frac{\mu_v}{\mu_0} = \frac{H}{\tau_s} \cdot \frac{\langle F_{fs} \rangle}{\langle F_N \rangle}, \quad (19)$$

Together with equations (12) and (14) to (16), the friction force was lowered under the applied ultrasonic vibration, or namely the variation of friction coefficient ratio μ_v/μ_0 was related to the amplitude and the acoustic softening effect parameter α. The applied ultrasonic vibration caused a softening effect inside the materials and softened the micro asperities on the contact surface to some extent, so the contact surface slip

shear force τ_s changed under the normal force. According to equation (11), this will directly affect the instant friction force $F_{fs}(t)$, and it was related in a certain way with α, amplitude ξ and slip sticking.

According to the above derivation based on the contact friction theoretical model, the functional relations between the tested parameters and friction coefficient were calculated, and the parameters involved in the theoretical model were determined. In equation (4), the vibration-free normal load $F_{N,0}$ can be directly measured by the electronic universal tensile testing machine. The hardness H of the soft material between two contact surfaces can be detected from hardness experiments. The stress increment ΔF induced by the out-of-plane normal ultrasonic vibration was determined. Together with Section 2, the k_t, ξ and ω were identified; the shear stress τ_s and the acoustic softening effect parameter α were obtained from the research findings about the volume effect[22].

4 Results and discussion

4.1 Effect of deep-drawing speed

When the punch radius was R0.3 and thickness was 0.1 mm, the friction coefficients at low and high deep drawing speeds (0.1, 10 mm/s) were measured (Fig. 7).

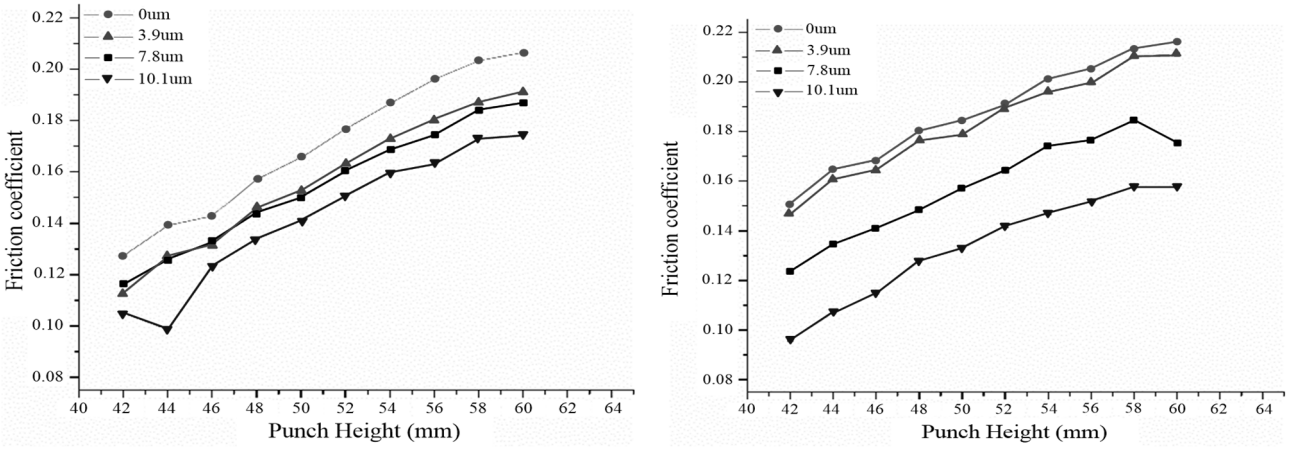

a) 0.1mm/s *b) 10mm/s*

Fig. 7 *Friction coefficient under different drawing speed*

As shown in Fig. 7, the applied ultrasonic vibration significantly affected the friction coefficients under both deep drawing speeds (0.1 and 10 mm/s). The change of friction coefficient curve in Fig. 7b is gentler than that in Fig. 7a. This was mainly because (1) the increased drawing speed led to a shorter contact time between punch molds and specimens, which lowered the various accumulative effects on the contact surface, and (2) the smaller molecular attraction between contact surfaces resulted in a smaller friction coefficient. As the ultrasonic vibration amplitude rose, the friction coefficient decreased, and the decreased value at low velocity was approximately uniformly distributed, but at high drawing velocity, the effects of vibration amplitudes on the decreased values of friction coefficient were largely different. At the same drawing height, the friction coefficients at the amplitudes of 7.8 um and 10.1 um at drawing velocity of 0.1 mm/s and 10 mm/s decreased by 6.7% and 18.8% respectively.

4.2 Effect of punch radius

The punch radius affected the friction and bending deformation during drawing forming to some extent. Hence, the effects of 3 punch radii (R0.3, R0.75, R1.5) on the friction coefficient were studied.

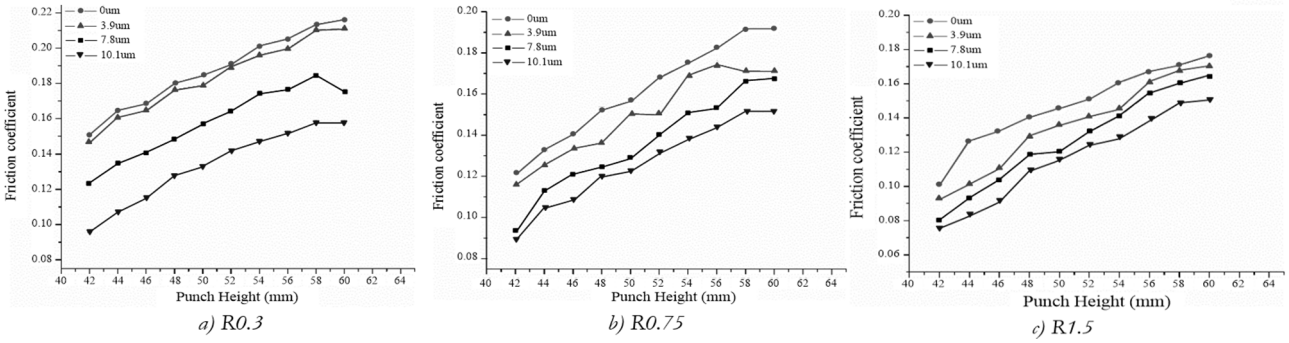

a) R0.3 *b) R0.75* *c) R1.5*

Fig. 8 *Friction coefficient under different punch fillet radius*

Clearly, the punch radius significantly affected the friction coefficient (Fig. 8). As the punch radius rose, the friction coefficient declined. Without the ultrasonic vibration, the friction coefficients at drawing height of 50 mm corresponding to R0.3 and R1.5 were 0.18 and 0.12 respectively. With the vibration at amplitude of 10.1 um, the friction coefficients became 0.13 and 0.11 respectively, indicating the applied ultrasonic vibration more sensitively affected the smaller punch radius.

4.3 Effects of thickness

During practical drawing forming, the bending deformation differs along with the sheet thickness. The differences in thickness induce additional pull forces to the middle and straight- wall parts of sheets, thereby affecting the friction coefficient. When the pull force caused by bending deformation during deep drawing is considered, the friction coefficient can be expressed as [21]:

$$\mu_e' = \frac{1}{\beta}\ln\frac{P_1-\Delta P}{P_2+\Delta P}, \quad (20)$$

Where:

ΔP…Additional pulling force induced by bending deformation.

As shown in Fig. 9, at the drawing speed of 0.1 mm/s and punch radius R0.3, the friction coefficients at the thickness of 0.2 mm were always smaller compared with the thickness of 0.1 mm, whether ultrasonic vibration was applied or not. Thinner specimens were more prone to bending deformation and at this time, the additional pulling forces at the middle part and at both sides of straight walls were small. According to equation (19), the resulting friction coefficients were larger than at the thickness of 0.2 mm, so the experimental results are consistent with theoretical results.

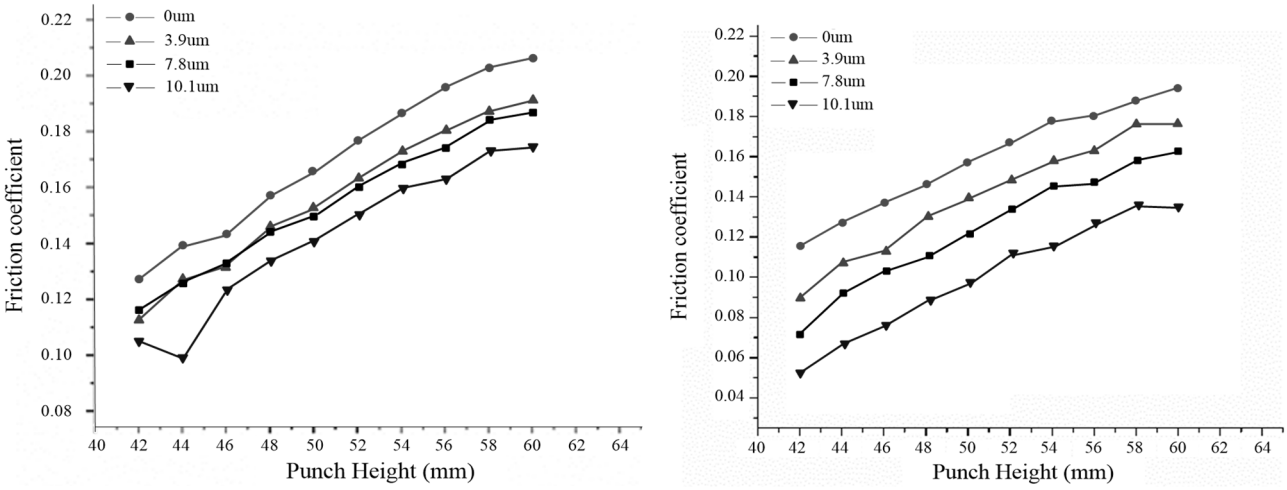

a) thickness 0.1mm *b) thickness 0.2mm*

Fig. 9 *Friction coefficient under different thickness*

4.4 Verification of the theoretical model for friction coefficient

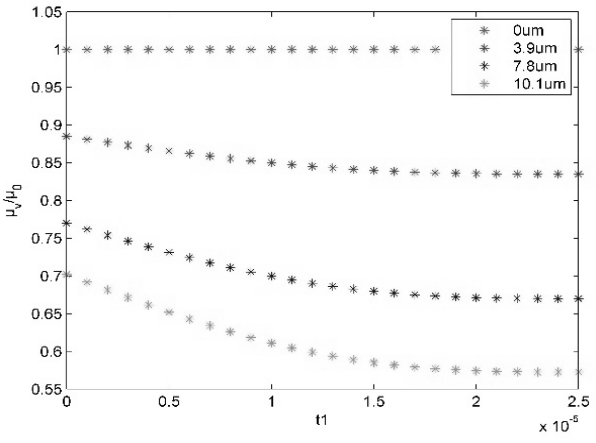

Fig. 10 *Relative friction coefficient based on contact friction theory model*

Based on the experimental parameters and results in Section 2, the parameters involved in the contact friction theoretical model in Section 3 were identified to further explore the relation between the theoretical model and ultrasonic vibration. The rated excited frequency of the applied ultrasonic vibration was 19.891 kHz, its peak power output was 2 kW, and the amplitude parameters were listed in Tab.1. The contact friction theoretical model established in Section 3 was programmed on Matlab.

The calculations from the contact friction model in Figure 10 showed that ultrasonic vibration significantly affected contact friction. The ratio of average friction coefficient μ_v to vibration- free friction coefficient μ_0 was 1, indicating the two friction coefficients were the same. After ultrasonic vibration was applied, the ratio of μ_v to μ_0 was < 1, indicating μ_v was smaller than μ_0, and the ratio declined with the

rise of amplitude ξ. Moreover, the ratio of μ_v/μ_0 was inversely proportional to the prolonging of X-axis time t_1, indicating the friction coefficient decreased with the increase of drawing speed. The above computation based on contact friction theoretical model is consistent with the experimental results.

To further discuss the precision of the contact friction theoretical model, we measured the friction coefficient of specimen SUS304 in thickness of 0.1 mm and drawing speed of 0.1 mm/s and recorded the parameters at drawing height of 60 mm, which will provide calculating parameters for the contact friction theoretical model. The experimental data were listed in Tab. 2.

Tab. 2 *Experimental values of friction coefficient*

Parameters	Vibration amplitude			
	0um	3.9um	7.8um	10.1um
Friction coefficient	0.216	0.191	0.187	0.174
Equivalent pressure (N)	645	605	587	523

The equivalent compressive force at varying amplitudes, or namely the normal pressure, ultrasonic vibration frequency and amplitude of the theoretical model were substituted into the contact friction theoretical equation (18) to determine the ratio i of μ_v/μ_0 (Tab. 3).

Tab. 3 *Calculation results of the ratio i*

Parameters	Vibration amplitude			
	0um	3.9um	7.8um	10.1um
i	1	0.885	0.7699	0.7021

The slide friction coefficient of specimen SUS304 was 0.25. Then based on the calculated results, the theoretical and measured data of contact friction coefficients were compared.

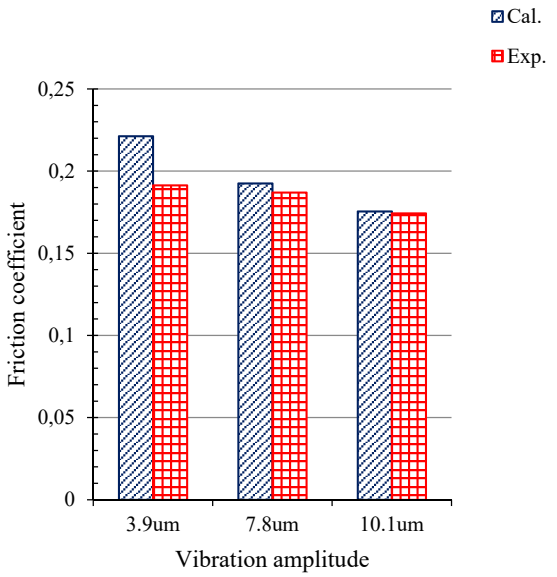

Fig. 11 *Comparison between the calculated and experimental values of friction coefficient*

As shown in Fig. 11, comparison shows the calculated values generally surpass the experimental values, and the differences between the two decrease with the increment of vibration amplitude, indicating the calculated values are closer to the experimental values and the theoretical model and experimental results are basically consistent. This comparison validates the accuracy of the friction coefficient theoretical model set up in Section 2.

4.5 Effects of vibration amplitude on surface morphology

After the experiments, surface morphology were taken using a scanning electron microscope to measure the surface quality. Results indicated the ultrasonic excitation improved the surface quality of specimens SUS304. The experiment results of specimens SUS304 with the vibration amplitude without ultrasonic vibration, and with ultrasonic vibration 3.9um, 7.8um and 10.1um for the thickness of 0.1mm and drawing speed of 0.1 mm/s are presented in Fig. 12.

As shown in Fig. 12, it is easy to notice that the surface deformed after applying ultrasonic vibration and surface is smoother, and the surface roughness is decreasing exponentially with vibration amplitude. The results show that the volume effect of ultrasonic vibration can also soften the surface of metal, which makes the surface of micro asperities easier to be flattened.

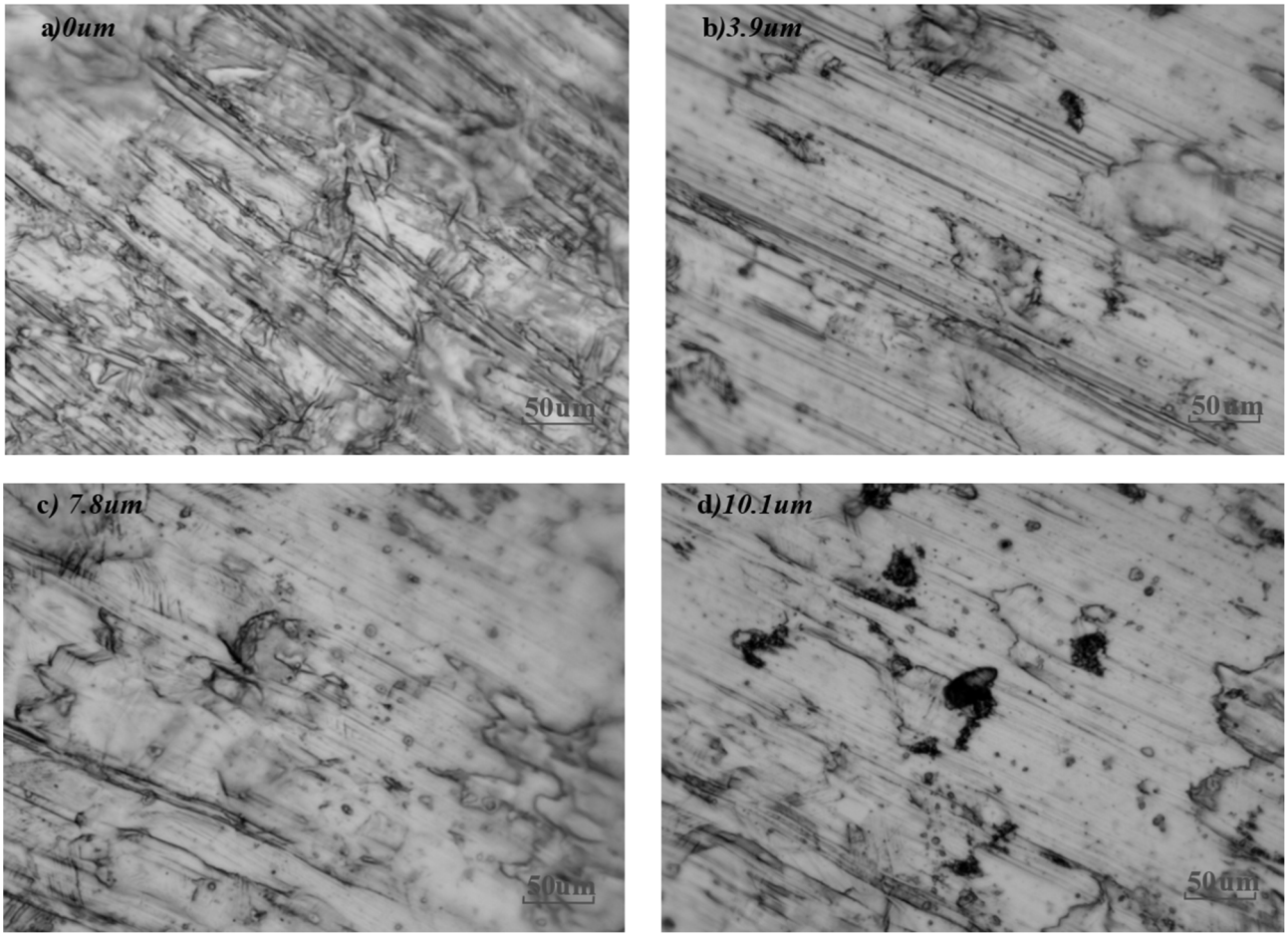

Fig. 12 *Surface micrographs at different vibration amplitude*

5 Conclusions

The effects of punch radius, deep-drawing speed and amplitude on the friction coefficient were studied on a friction coefficient measurement platform assisted by ultrasonic vibration. A contact friction model based on the tribology theory of adhesion and plowing was constructed and used to explain the friction reduction phenomenon of applied out-of-plane normal vibration. Together with experimental results, relevant parameters of the theoretical model were calibrated and used to analyze modeling precision.

- (1) The deep-drawing speed significantly affected the friction coefficient, and the friction coefficient curve at a larger speed changed more gently when other experimental parameters were the same. As the ultrasonic vibration amplitude rose, the friction coefficient decreased, and the decreased value at low drawing speed was almost uniformly distributed, but at high drawing speed, the effects of vibration amplitudes on the decreased values of friction coefficient were largely different. At the same drawing height, the friction coefficients at the amplitudes of 7.8 um and 10.1 um at drawing speed of 0.1 mm/s and 10 mm/s decreased by 6.7% and 18.8% respectively.
- (2) With the absence of ultrasonic vibration, the friction coefficients at drawing height of 50 mm corresponding to R0.3 and R1.5 were 0.18 and 0.12 respectively. After the vibration at amplitude of 10.1 um was applied, the friction coefficients became 0.13 and 0.11 respectively, indicating the effect of the applied ultrasonic vibration was more sensitive at the smaller punch radius.
- (3) When other experimental parameters were the same, since thinner specimens were more prone to bending deformation, the additional pulling forces at the middle and at two sides of straight walls were small and consequently, the friction coefficients of thinner specimens surpassed those of thicker specimens whether ultrasonic vibration was applied or not.

- (4) Theoretical model showed the average friction coefficient μ_v was smaller than the vibration-free friction coefficient μ_0, and the μ_v/μ_0 ratio declined with the increment of amplitude. The μ_v/μ_0 ratio was inversely proportional to the prolonging of X-axis time t_1, indicating the coefficient decreased with the increase of the drawing speed and the calculated values are consistent with the experimental results.
- (5) Different vibration amplitudes have significant influence on the surface morphology of metal. The surface becomes smoother and with the increase of vibration amplitude, and the surface roughness is decreasing exponentially with vibration amplitude.

Acknowledgment

The authors gratefully acknowledge the supports of the Natural Science Foundation of Educational Commission of Anhui Province of China (Grant No. KJ2019A0576) and the project of the open competition mechanism to select the best candidates (Grant No. 220015).

References

[1] LI Z., YANG D., HAO W.,et al. (2016). A novel technique for micro-hole forming on skull with the assistance of ultrasonic vibration. *Journal of the Mechanical Behavior of Biomedical Materials*, 57: 1-13

[2] KRIECHENBAUER S., MAUERMANN R., MULLER P. (2014). Deep Drawing with Superimposed Low-frequency Vibrations on Servo-screw Presses. *Procedia Engineering*, 81: 905-913

[3] ŘIHÁČEK J, PODANÝ K, FALTÝNEK F. (2019). Prediction of the Stamped Part Thinning Depending on Its Geometry and Blank Material. *Manufacturing Technology*, 19: 314-320

[4] LIU S., SHAN X., GUO K., et al. (2018). Experimental study on titanium wire drawing with ultrasonic vibration. *Ultrasonics*, 83: 60-67

[5] MICHNA Š, HREN I, CAIS J, et al. (2020). The Research of the Different Properties and Production Parameters having Influence on Deep-Drawing Sheets made of AlMg3 Alloy. *Manufacturing Technology*, 20: 347-354

[6] LIU Y., SUSLOV S., HAN Q., et al. (2013). Comparison Between Ultrasonic Vibration-Assisted Upsetting and Conventional Upsetting. *Metallurgical and Materials Transactions A-Physical Metallurgy and Materials Science*, 3232: 1-13

[7] RASOLI M.A., ABDULLAH A., FARZIN M., et al. (2012). Influence of ultrasonic vibrations on tube spinning process. *Journal of Materials Processing Technology*, 212: 1443-1452

[8] TAN R., ZHAO X., GUO S., et al. (2020). Sustainable production of dry-ultra-precision machining of Ti–6Al–4V alloy using PCD tool under ultrasonic elliptical vibration-assisted cutting. *Journal of Cleaner Production,* 248: 1-44

[9] ZHU L., NI C., YANG Z., et al. (2019). Investigations of micro-textured surface generation mechanism and tribological properties in ultrasonic vibration-assisted milling of Ti–6Al–4V. *Precision Engineering*, 57: 229-243

[10] GUNDUZ I.E., MCCLAIN M., CATTANI P., et al. (2018). 3D printing of extremely viscous materials using ultrasonic vibrations. *Additive Manufacturing*, 22: 98-103

[11] SIEGERT K., ULMER J. (2001). Influencing the Friction in Metal Forming Processes by Superimposing Ultrasonic Waves. *Cirp Annals-Manufacturing Technology,* 50: 195-200

[12] BUNGET C., NGAILE G. (2011). Influence of ultrasonic vibration on micro-extrusion. *Ultrasonics*, 51: 606-616

[13] YAO Z., KIM G.Y., FAIDLEY L., et al. (2012). Effects of superimposed high-frequency vibration on deformation of aluminum in micro/meso-scale upsetting. *Journal of Materials Processing Technology,* 212: 640-646

[14] HUNG J.C., HUANG C.C. (2012). Evaluation of friction in ultrasonic vibration-assisted press forging using double cup extrusion tests. *International Journal of Precision Engineering and Manufacturing*, 13: 2103-2108

[15] TSAI C.C., TSENG C.H. (2006). The effect of friction reduction in the presence of in-plane vibrations. *Archive of Applied Mechanics*, 75: 164-176

[16] POPOV M., POPOV V.L., POPOV N.V. (2017). Reduction of friction by normal oscillations. I. Influence of contact stiffness. *Friction*,5: 45-55

[17] MAO X., POPOV V.L., STARCEVIC J., et al. (2017). Reduction of friction by normal oscillations. II. In-plane system dynamics. *Friction,* 5: 194-206

[18] POPOV M. (2016). Critical velocity of controllability of sliding friction by normal oscillations in viscoelastic contacts. *Mechanical Engineering,* 14: 335–341

[19] POPOV V.L., POHRT R., HESS M. (2016). General procedure for solution of contact problems under dynamic normal and tangential loading based on the known solution of normal contact problem. *Journal of Strain Analysis for Engineering Design*, 51: 1-9

[20] TEIDELT E., WILLERT E., FILIPPOV A.E., et al.L (2012). Modeling of the dynamic contact in stick-slip microdrives using the method of reduction of dimensionality. *Physical Mesomechanics*, 15: 287-292

[21] WANG W., WAGONER R.H., WANG X.J. (1996). Measurement of friction under sheet forming conditions. *Metallurgical and Materials Transactions A-Physical Metallurgy and Materials Science,* 27: 3971-3981

[22] ZHA C.L., CHEN W. (2019). Theories and experiments on effects of acoustic energy field in micro-square cup drawing. *International Journal of Advanced Manufacturing Technology*, 104: 4791–4802

[23] ARCHIE H., WILLIAM B.S. (1949). Engineering mechanics, New York, Prentice-Hall, Inc 249: 0-505

[24] HU J., SHIMIZU T., YANG M. (2018). Investigation on ultrasonic volume effects: Stress superposition, acoustic softening and dynamic impact. *Ultrasonics Sonochemistry*, 48: 240-248

[25] WANG C.J., LIU Y., GUO B., et al. (2016). Acoustic softening and stress superposition in ultrasonic vibration assisted uniaxial tension of copper foil: experiments and modeling. *Materials and Design*, 112: 246–253

[26] BOWDEN F.P., TABOR D.F. (1964). The friction and Lubrication of Solids. *Wear* ,7: 557-558